Minimum heat transfer by laminar natural convection across a laterally heated vertical slot

P. G. Daniels
Department of Mathematics, City University, London, UK

Solutions for the convective regime in a laterally heated vertical slot provide a prediction of the gap width for which the heat transfer across the slot is minimized. Although the theory applies strictly for large Prandtl numbers, it provides a reasonable approximation for air when multicellular convection is weak or nonexistent. Comparisons with numerical and experimental results confirm this assertion.

Keywords: heat transfer; natural convection; cavity wall insulation

Introduction

In the Boussinesq approximation, heat transfer across a vertical slot whose sides are held at different constant temperatures depends on three nondimensional parameters: a Rayleigh number based on the temperature difference, the Prandtl number of the fluid filling the slot, and the aspect ratio of the slot. Batchelor[1] argued that for sufficiently narrow slots the total heat transfer would be large, because it is primarily due to lateral conduction and therefore inversely proportional to the slot width. Conversely, for sufficiently wide slots the increased freedom of movement of the fluid would lead to the enhanced transfer of heat by convection, suggesting the possibility of a critical width l^* for which the total transfer is a minimum. The determination of such a critical value is of obvious importance in the thermal insulation of buildings by cavity wall or window insulation.

The equations governing steady two-dimensional (2-D) motions of the fluid may be written as

$$\nabla^4\psi - \mathrm{Ra}_h \frac{\partial T}{\partial x} = \frac{1}{\mathrm{Pr}} \frac{\partial(\nabla^2\psi, \psi)}{\partial(x, z)} \tag{1}$$

$$\nabla^2 T = \frac{\partial(T, \psi)}{\partial(x, z)} \tag{2}$$

where the temperature T and stream function ψ are made nondimensional by the temperature difference across the slot ΔT^* and the thermal diffusivity κ. The coordinates x and z are made nondimensional by the slot height h^*, with the cold wall located at $x=0$ and the hot wall at $x=L$, where $L=l^*/h^*$ is the aspect ratio. Assuming that the horizontal surfaces $z=0$ and $z=1$ are adiabatic, it follows that the boundary conditions on the walls of the slot are

$$\psi = \frac{\partial\psi}{\partial x} = 0 \qquad (x=0, x=L) \tag{3}$$

$$T=0 \quad (x=0) \quad \text{and} \quad T=1 \quad (x=L) \tag{4}$$

$$\psi = \frac{\partial\psi}{\partial z} = \frac{\partial T}{\partial z} = 0 \qquad (z=0, z=1) \tag{5}$$

Address reprint requests to Professor Daniels at the Department of Mathematics, City University, Northampton Square, London EC1V 0HB, UK.

Received 20 April 1989; accepted 14 March 1990

The parameters appearing in Equation 1 are the Prandtl number $\mathrm{Pr}=\nu/\kappa$ and the Rayleigh number $\mathrm{Ra}_h=\alpha^* g\,\Delta T^* h^{*3}/\kappa\nu$, where α^* is the coefficient of thermal expansion and ν is the kinematic viscosity.

An appropriate nondimensional measure of total heat transfer is a Nusselt number for the cold wall:

$$\overline{\mathrm{Nu}} = \int_0^1 \frac{\partial T}{\partial x}(0, z)\, dz \tag{6}$$

In insulating-system applications, the main interest is the dependence of $\overline{\mathrm{Nu}}$ on l^* for given values of ΔT^*, h^*, and the material properties of the fluid. Equations 1–6 show that, in general, $\overline{\mathrm{Nu}}$ is a function of Ra_h, L, and Pr and—as variations in l^* are confined to the single parameter L—the main objective is to determine the critical value $L=L_c(\mathrm{Ra}_h, \mathrm{Pr})$ at which $\overline{\mathrm{Nu}}$ is a minimum for given values of Ra_h and Pr. This result might be achieved by extensive numerical calculations of the type described by Catton *et al.*[2] and Lee and Korpela,[3] who have made some progress in the investigation of the three-dimensional (3-D) parameter space involved. Here it is argued that a simple formula can be used to obtain a good approximation to L_c for a wide range of values of Ra_h and Pr of practical interest.

Variation of the Nusselt number in the convective regime

A basic assumption of the present theory is that the aspect ratio L is small, in which case three main flow regimes can be identified. For Rayleigh numbers $\mathrm{Ra}_h \lesssim L^{-3}$, heat is transferred across the slot mainly by conduction, and the horizontal temperature gradient drives a vertical two-way flow up the hot side and down the cold side. At higher Rayleigh numbers $\mathrm{Ra}_h \sim L^{-4}$, the flow enters a convective regime in which neither the isotherms nor the streamlines are parallel to the vertical walls. Heat is no longer transferred across the slot predominantly by conduction. Finally, for Rayleigh numbers $\mathrm{Ra}_h \gg L^{-4}$, the flow develops a boundary-layer structure with most of the vertical motion adjacent to the side walls of the slot. At large Prandtl numbers the transition from the conductive to the convective regime takes the form of an inward penetration of nonparallel effects associated with the turning motions at the ends of the slot.[4] At lower Prandtl numbers a more rapid transition can occur in which instability leads to the occurrence of multiple rolls superimposed on the large-scale circulation.

The influence of multiple-roll instability is discussed in later sections.

Both the conductive and boundary-layer regimes emerge as limiting forms of the convective regime where, in the formal limit of infinite Prandtl number, the flow throughout most of the slot can be found by utilizing a "vertical boundary-layer" approximation[5] in which:

$$\psi \sim \mathrm{Ra}_h^{1/4}\Psi(X, z) \qquad T \sim \Theta(X, z) \tag{7}$$

where $x = \mathrm{Ra}_h^{-1/4}X$. The full set of governing equations and boundary conditions, Equations 1–5, reduces to the simplified form:

$$\frac{\partial^4\Psi}{\partial X^4} = \frac{\partial\Theta}{\partial X} \quad \text{and} \quad \frac{\partial^2\Theta}{\partial X^2} = \frac{\partial(\Theta, \Psi)}{\partial(X, z)} \tag{8}$$

$$\Psi = \frac{\partial\Psi}{\partial X} = 0 \qquad (X = 0, X = l) \tag{9}$$

$$\Theta = 0 \qquad (X = 0) \quad \text{and} \quad \Theta = 1 \qquad (X = l) \tag{10}$$

where

$$l = \mathrm{Ra}_h^{1/4}L \tag{11}$$

The conductive limit corresponds to $l \to 0$ and the boundary-layer limit to $l \to \infty$. The nature of the vertical boundary-layer approximation is such that the full boundary conditions at $z = 0$ and $z = 1$, Equation 5, can no longer be satisfied. Instead a zero mass–flux condition

$$\Psi = 0 \qquad (z = 0, z = 1) \tag{12}$$

is assumed. This assumption is consistent with a local asymptotic solution[5,6] of the system of Equations 8–10 as $z \to 0$ and $z \to 1$. The corresponding horizontal boundary-layer structures needed to adjust the solution to the wall conditions, Equation 5, have been discussed in Reference 7. Whether condition 12 is too stringent for the vertical boundary-layer system is difficult to determine. However, in the boundary-layer regime, approximate solutions satisfying this type of condition have been obtained by both Oseen and integral techniques.[8,9]

The system of Equations 8–12 depends only on the "convective" parameter l, so the Nusselt number is given to leading order by

$$\overline{\mathrm{Nu}} \sim \mathrm{Ra}_h^{1/4}\mathrm{Nu}(l) \tag{13}$$

where

$$\mathrm{Nu}(l) = \int_0^1 \frac{\partial\Theta}{\partial X}(0, z)\, dz \tag{14}$$

Numerical investigation of the system[5] using a spectral decomposition in z and central differences in X yields solutions for $\mathrm{Nu}(l)$ that confirm Batchelor's original assertion of a position of minimum heat transfer. This position occurs when:

$$l = l_c \approx 4.5 \quad \text{and} \quad \mathrm{Nu} = \mathrm{Nu}_c \approx 0.29 \tag{15}$$

Theoretical confirmation of these results can be obtained from an analysis of the limit as l tends to zero. The solution of the system of Equations 8–12 then consists of a conduction-dominated core region $0 < z < 1$ with:

$$\Psi \sim l^3\Psi_c(\bar{x}) = l^3\frac{\bar{x}^2}{24}(1 - \bar{x})^2 \quad \text{and} \quad \Theta \sim \Theta_c(\bar{x}) = \bar{x} \tag{16}$$

where $\bar{x} = X/l$. The end conditions 12 require that the vertical flow associated with Ψ_c be turned so that near $z = 0$, for example, there is a local adjustment on a vertical scale $\bar{z} = z/l^4 = \mathrm{O}(1)$, where the solution can be written as

$$\Psi \sim l^3\bar{\Psi}(\bar{x}, \bar{z}) \quad \text{and} \quad \Theta \sim \bar{\Theta}(\bar{x}, \bar{z}) \tag{17}$$

Here $\bar{\Psi}$ and $\bar{\Theta}$ satisfy the full equations and boundary conditions 8–10 (with Ψ, Θ, z, X, and l replaced by $\bar{\Psi}$, $\bar{\Theta}$, $\bar{z}$, $\bar{x}$, and 1, respectively). An approximate solution can be found by expanding about the form as $\bar{z} \to \infty$, which must join smoothly with the core solution, giving

$$\bar{\Psi} = \Psi_c(\bar{x}) + a\phi(\bar{x})e^{-\mu\bar{z}} \quad \text{and} \quad \bar{\Theta} = \Theta_c(\bar{x}) + a\theta(\bar{x})e^{-\mu\bar{z}} \tag{18}$$

where a is a constant. Here μ, ϕ, and θ are the leading eigenvalue and eigenfunctions of the system:

$$\left.\begin{aligned} &\phi^{\mathrm{IV}} = \theta' \quad \text{and} \quad \theta'' = \mu(\Psi_c'\theta - \Theta_c'\phi) \\ &\phi = \phi' = \theta = 0 \qquad (\bar{x} = 0, \bar{x} = 1) \end{aligned}\right\} \tag{19}$$

The eigenvalue with smallest real part is $\mu = 2.58 \times 10^3$. The corresponding eigenfunctions, which are shown in Reference 4, have the properties $\theta'(0) = 1.3$, $\theta'(1) = -4.4$, and $\phi_{\max} = 2.5 \times 10^{-3}$ when a normalization $\theta_{max} = 1$ is applied. Solutions (18) can be regarded as first terms in series expansions about $\bar{z} = \infty$, which could be improved by calculating nonlinear corrections and higher eigenfunctions. However the leading terms are probably sufficient to give a reliable indication of the nature of the flow; the function $\phi(\bar{x})$ has a nearly symmetric form not dissimilar to Ψ_c, suggesting that higher eigenfunctions that contains successively more zeros in the interval $0 < \bar{x} < 1$ play a relatively minor role.

The solution in the end region at the top of the slot is obtained from that given in Equation 18 by invoking the centro-symmetry of the flow,[8] equivalent to $\psi(x, z) = \psi(L - x, 1 - z)$, $T(x, z) = 1 - T(L - x, 1 - z)$ and the Nusselt number, Equation 14, can then be calculated from the main core contribution, Equation 16, together with the convective corrections arising from each end zone. Thus

$$\mathrm{Nu} \sim l^{-1} + l^3(\alpha + \beta) \qquad \text{as } l \to 0 \tag{20}$$

where

$$\left.\begin{aligned} \alpha &= \int_0^\infty \left(\frac{\partial\bar{\Theta}}{\partial\bar{x}}(1, \bar{z}) - 1\right) d\bar{z} = a\mu^{-1}\theta'(1) \\ \beta &= \int_0^\infty \left(\frac{\partial\bar{\Theta}}{\partial\bar{x}}(0, \bar{z}) - 1\right) d\bar{z} = a\mu^{-1}\theta'(0) \end{aligned}\right\} \tag{21}$$

Notation

g	Acceleration due to gravity
h^*	Slot height
l	Convective parameter
l^*	Slot width
L	Aspect ratio
$\overline{\mathrm{Nu}}$, Nu	Nusselt numbers
Pr	Prandtl number
Ra_h	Rayleigh number based on slot height
Ra_l	Rayleigh number based on slot width
T	Nondimensional temperature
ΔT^*	Temperature difference across slot
x, z	Nondimensional coordinates

Greek symbols

α^*	Coefficient of thermal expansion
Θ	Scaled temperature
κ	Thermal diffusivity
ν	Kinematic viscosity
ψ	Nondimensional stream function
Ψ	Scaled stream function

In addition, from integration of the energy Equation 8 over the end zone and use of the mass-flux condition 12,

$$\alpha-\beta=\int_0^1 \Psi_c\, d\bar{x}=\frac{1}{720} \tag{22}$$

so that

$$a=\mu\{720[\theta'(1)-\theta'(0)]\}^{-1}=-0.63 \tag{23}$$

An alternative—but less favorable method of estimating the value of a—is to apply Equation 12 directly to Equation 18, so that, for instance, comparing maximum values of ϕ and Ψ_c would give

$$a=\frac{-\Psi_c(\frac{1}{2})}{\phi_{\max}}\approx -1 \tag{24}$$

Then, however, solution 18 is used directly at $\bar{z}=0$, where it is likely to be least accurate. The value, given by Equation 23, is preferred, because it ensures an overall heat transfer balance and makes use of solution 18 where it is most relevant, incorporating the mass-flux condition 12 indirectly.

Figure 1 shows the numerical calculation of Nu(l) together with the two-term approximation 20 when a is determined by Equation 23, so that $\alpha+\beta=0.00076$. The curve corresponding to the alternative value of a given by Equation 24, for which $\alpha+\beta=0.0012$, is also shown for comparison. The still higher curve is that corresponding to Batchelor's supposition that $\beta=0$ and $\alpha=1/720$, where the convective heat transfer is assumed to occur solely at the base of the hot wall and the top of the cold wall. For the values $\alpha=0.0011$ and $\beta=-0.0003$ given by Equations 21 and 23, the heat transfer at the base of the cold wall is actually reduced relative to the conductive value. However, this transfer is outweighed by the enhanced transfer at the top of the wall, which is associated with a significant narrowing of the isotherms there.

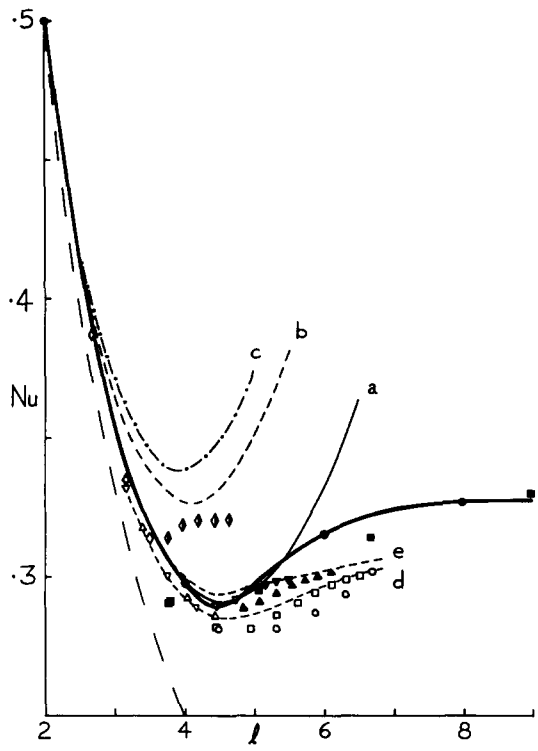

Figure 1 Scaled Nusselt number Nu as a function of the convective parameter l: spectral solution of the core problem[5] (—●—); one-term conductive approximation (——) and two-term approximation 20, with $\alpha+\beta$ equal to (a) 0.00076, (b) 0.0012, and (c) 1/720. Numerical data from Reference 2 is for Pr=∞, L=1/15 (■) and that from Reference 3 is for Pr=0.71 and L=1/5 (○), 1/10 (□), 1/15 (△), 1/20 (▽), and 1/40 (◇), with partial shading indicating the presence of multicellular convection. Additional dashed curves are from the numerical data of Reference 11 for Pr=0.71 and Ra_n equal to (d) 1.8×10^7 and (e) 7.1×10^7.

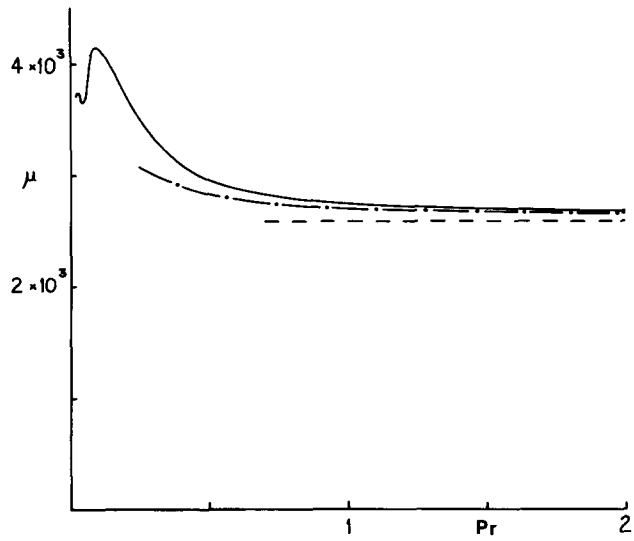

Figure 2 Influence of Prandtl number on the end-zone solution, showing the behavior of the leading eigenvalue μ: numerical solution by the Runge–Kutta technique (——); limit value 2,582 for Pr→∞ (– – –); and two-term asymptotic formula 32 (—·—). Note that for air μ=2,816.

Prandtl number effects

As the preceding results are based on the assumption of infinite Prandtl number, it is of interest to know how they are modified for finite values of practical significance—particularly for air, where Pr=0.71. An indication of the influence of the Prandtl number on Equations 21 and 23 can be obtained by retaining the appropriate inertia terms in the reduced vorticity equation, which becomes

$$\frac{\partial^4\Psi}{\partial X^4}=\frac{\partial\Theta}{\partial X}+\frac{1}{\mathrm{Pr}}\left(\frac{\partial^3\Psi}{\partial X^3}\frac{\partial\Psi}{\partial z}-\frac{\partial^3\Psi}{\partial X^2\,\partial z}\frac{\partial\Psi}{\partial X}\right) \tag{25}$$

At infinite Prandtl number, the leading eigenvalue of Equations 19 determines the vertical scale of the end region. From Equation 25, the solution of the corresponding system at finite Prandtl number is obtained by replacing the first of Equations 19 by

$$\phi^{\mathrm{IV}}=\theta'+\mu\mathrm{Pr}^{-1}(\Psi_c'\phi''-\Psi_c'''\phi) \tag{26}$$

The new solution for the leading eigenvalue is shown in Figure 2. Note that for air the value of μ is altered by less than 10% of its value for infinite Prandtl number. An asymptotic analysis of the system for Pr→∞, where the solution can be written as

$$\phi\sim\phi_0+\mathrm{Pr}^{-1}\phi_1 \qquad \theta\sim\theta_0+\mathrm{Pr}^{-1}\theta_1 \quad \text{and} \quad \mu\sim\mu_0+\mathrm{Pr}^{-1}\mu_1 \tag{27}$$

confirms the weak dependence on Prandtl number. At leading order, μ_0, ϕ_0, and θ_0 are the solutions of Equations 19, and the system for μ_1, ϕ_1, and θ_1,

$$\left.\begin{aligned}\phi_1^{\mathrm{IV}}-\theta_1'&=\mu_0(\Psi_c'\phi_0''-\Psi_c'''\phi_0)=\chi_1\\ \theta_1''-\mu_0(\Psi_c'\theta_1-\phi_1)&=\mu_1(\Psi_c'\theta_0-\phi_0)=\chi_2\end{aligned}\right\} \tag{28}$$

has a solution satisfying the appropriate boundary conditions only if:

$$\int_0^1 (\chi_1\bar{\phi}+\chi_2\bar{\theta})\,d\bar{x}=0 \tag{29}$$

where $\bar{\phi}$ and $\bar{\theta}$ are solutions of the adjoint system:

$$\left.\begin{aligned}\bar{\phi}^{IV}&=-\mu_0\bar{\theta} \qquad \bar{\theta}'=\mu_0\Psi_c''\bar{\theta}-\bar{\phi}'\\ \bar{\phi}&=\bar{\phi}'=\bar{\theta}=0 \qquad (\bar{x}=0,\,\bar{x}=1)\end{aligned}\right\} \tag{30}$$

Thus

$$\mu_1=\frac{-\mu_0\int_0^1(\Psi_c'\phi_0''-\Psi_c'''\phi_0)\bar{\phi}\,d\bar{x}}{\int_0^1(\Psi_c'\theta_0-\phi_0)\bar{\theta}\,d\bar{x}} \tag{31}$$

For the leading eigenvalue a numerical solution gives $\mu_1=122.3$, so that:

$$\mu\sim 2{,}582+122.3\mathrm{Pr}^{-1} \qquad (\mathrm{Pr}\to\infty) \tag{32}$$

This result is shown in Figure 2.

Comparison with experimental and numerical results

These arguments suggest that comparing the theoretical prediction, Equation 15, with experimental and numerical data is worthwhile even for a fluid of relatively low Prandtl number. Experimental results for air[10] are largely in line with the comprehensive set of numerical data obtained in Reference 3 and so—in Figure 1—the main comparison is with the latter results. Most data points do fall close to the universal curve Nu(l) given by the spectral solution of the reduced system. Moreover, results for infinite Prandtl number obtained in Reference 2 fit well over a wide range of l values. Data for air given in Reference 3 are displayed in sets of constant aspect ratio L, from which it is observed that only those for the smallest aspect ratio, $L=1/40$, deviate significantly from the minimum predicted by Equation 15. Results for constant L correspond to different values of Ra_h so the minimum associated with the data points for $L=1/40$ is *not* a significant one. Curves at constant Ra_h must be constructed in order for any minimum associated with an optimum slot width to be observable. Further results reported by Korpela, Lee, and Drummond[11] allow these curves to be constructed for several values of Ra_h, including the two extreme values 1.8×10^7 and 7.1×10^7 shown in Figure 1. Results are not available for the much higher values of Ra_h corresponding to $L=1/40$, and the position of any minimum in these cases remains undetermined.

Multicellular convection

The discrepancy between the formula (20) and the numerical results for $L=1/40$ appears to be due to multicellular convection, the presence of which is indicated by the partially shaded data points in Figure 1. Results of a weakly nonlinear theory[12] for $\mathrm{Pr}=7.5$ indicate only a small change in the conductive Nusselt number at the onset of this stationary instability. However, it seems reasonable to believe that in such cases the sudden enhancement of convection will produce a minimum higher than that given by Equation 15 but lower than (or possibly equal to) the value of the Nusselt number at the onset of instability. It is argued here that the Prandtl number does not have a significant influence on the large-scale convective flow until its value is somewhat less than that for air. The formal assumption of infinite Prandtl number means that multiple rolls associated with shorter length-scale instabilities are avoided.

In practice, however, the conductive state, Equation 16, is subject to stationary instability[13] unless the Rayleigh number based on slot width, $\mathrm{Ra}_l=\mathrm{Ra}_hL^3$, satisfies

$$\mathrm{Ra}_l<\mathrm{Ra}_{l,S}(\mathrm{Pr})\approx 7.9\times10^3\mathrm{Pr} \tag{33}$$

and a time-dependent instability[14,15] unless it satisfies

$$\mathrm{Ra}_l<\mathrm{Ra}_{l,T}(\mathrm{Pr}) \tag{34}$$

where $\mathrm{Ra}_{l,T}\sim 9.4\times10^3\mathrm{Pr}^{1/2}$ as $\mathrm{Pr}\to\infty$. At finite Prandtl numbers the stationary instability must be taken into account, even in the description of the base flow in the slot.[4]

If the stability criterion, condition 33, associated with the conductive state remained uninfluenced by the underlying change in the large-scale flow of the convective regime, multicellular convection would occur at a value of l less than l_c if:

$$L<\frac{l_c^4}{7.9\times10^3\mathrm{Pr}}=\frac{0.052}{\mathrm{Pr}} \tag{35}$$

In this case the sudden enhancement of convection throughout the slot would lead to the possibility of a discontinuity in the gradient of the Nusselt number curve of Figure 1 at

$$l=l_s=10\left(\frac{7.9\mathrm{Pr}}{\mathrm{Ra}_h^{1/4}}\right)^{1/3} \qquad (<l_c) \tag{36}$$

A weakly nonlinear theory in the neighborhood of l_s would be required to determine the range of values of $\mathrm{Pr}/\mathrm{Ra}_h^{1/4}$(0 for which the gradient of Nu is positive for $l>l_s$, in which case l_s itself would become the position of minimum heat transfer. However, whether applying the results at lower Pr values in such a nonlinear theory for large Prandtl numbers would still be relevant remains unclear.

In Equation 36 it is assumed that the conductive stability criterion is not affected by convective changes in the large-scale flow. This assumption is quite good for the range of interest ($l<l_c$), because l_c happens to be near the lower end of the convective regime.[5] However, an improved stability criterion can be obtained from Bergholz.[16] This suggests that, for the range $l<l_c$ and Prandtl numbers less than about 10 (in order to exclude traveling-wave instabilities), condition 33 can be replaced by $\mathrm{Ra}_l<\mathrm{Ra}_{l,S}$ where:

$$\frac{\mathrm{Ra}_{l,S}}{\mathrm{Pr}}=7.9\times10^3+kl^4 \tag{37}$$

The value $k=6$ gives a reasonable fit with the results of Reference 16. The large-scale convective flow is a stabilizing influence, with the result that condition 35 is modified to become:

$$L<(7.9\times10^3l_c^{-4}+k)^{-1}\mathrm{Pr}^{-1}=\frac{0.040}{\mathrm{Pr}} \tag{38}$$

The value of l_s is now determined as the smaller of the two real roots of the quartic equation:

$$l_s^4-\mathrm{Ra}_h^{1/4}(k\mathrm{Pr})^{-1}l_s^3+7.9\times10^3k^{-1}=0 \tag{39}$$

and is shown in Figure 3, along with the cruder approximation given by Equation 36. Now $l_s<l_c$ for:

$$\frac{\mathrm{Pr}}{\mathrm{Ra}_h^{1/4}}<0.0088 \tag{40}$$

In this case the heat transfer minimum is likely to be influenced by multicellular convection. The optimum slot width then probably lies between that corresponding to $l=l_s$ and that corresponding to $l=l_c$. Figure 4 shows the scaled Nusselt number Nu associated with each of the curves $l=l_s$ and $l=l_c$. The corresponding absolute Nusselt number $\overline{\mathrm{Nu}}$ shows how the overall optimum heat transfer level is influenced by external

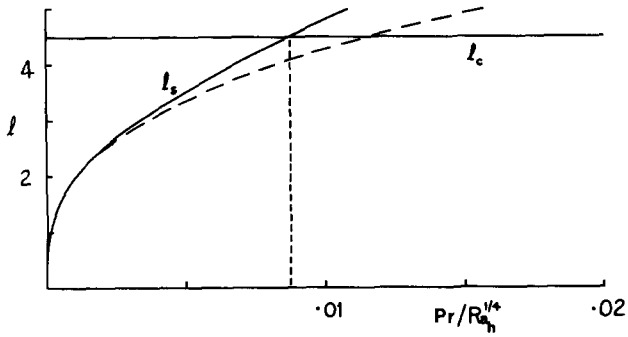

Figure 3 Values of l associated with the point of minimum heat transfer (l_c) and the onset of multicellular convection (l_s). In the latter case both the conductive approximation, Equation 36 (---), and the improved approximation, Equation 39 (——) are shown.

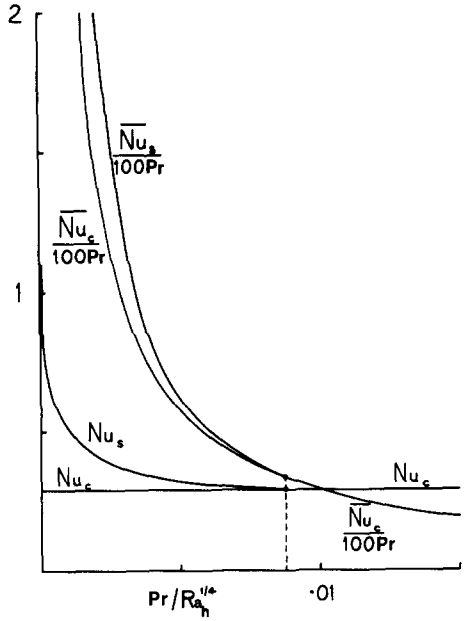

Figure 4 Values of the scaled Nusselt number Nu associated with the point of minimum heat transfer (Nu$_c$) and the onset of multicellular convection (Nu$_s$). The corresponding absolute Nusselt numbers $\overline{Nu}_c$ and $\overline{Nu}_s$ are also shown.

conditions, as imposed by the values of Pr and Ra_h. When inequality 40 is satisfied, $\overline{Nu}_s$ and $\overline{Nu}_c$ likely provide bounds on the optimum level of heat transfer.

Conclusions

The present results indicate that, for large Prandtl number fluids, heat transfer across a vertical slot is minimized when the aspect ratio $L \sim Ra_h^{-1/4} l_c \approx 4.5 Ra_h^{-1/4}$, that is, for a slot width of:

$$l_c^* \approx 4.5\left(\frac{\kappa\nu h^*}{\alpha^* g\,\Delta T^*}\right)^{1/4} \tag{41}$$

at which the nondimensional Nusselt number is

$$\overline{Nu} \approx 0.29\left(\frac{\alpha^* g\,\Delta T^*\, h^{*3}}{\kappa\nu}\right)^{1/4} \tag{42}$$

Although these results are formally valid in the limit of infinite Prandtl number, they appear to provide excellent approximations for fluids of Prandtl number as low as that for air unless multicellular convection is present. In that case the results are modified in a manner that depends on the ratio $Pr/Ra_h^{1/4}$ and are summarized in Figures 3 and 4.

These conclusions may be confirmed by reference to the numerical data for air given in Figure 1. In this case the critical aspect ratio given by condition 38 is $L = 0.056$, which is consistent with a good approximation to the universal position of minimum heat transfer, Equation 41, for those data sets for which $L \geq 1/20$. The Nusselt number is close to the value given by Equation 42. For $L = 1/40$, multicellular convection occurs at $l \approx 3.6$, well ahead of the universal minimum and in line with the value $l_s = 3.54$ given by the solution of Equation 39, with $Pr = 0.71$ and $Ra_h^{-1/4} l_s = L = 1/40$. The corresponding value of the Nusselt number is accurately given by formula 20.

In applications to typical double-glazing systems, it appears likely that multicellular convection must be taken into account. For a temperature difference of 5°C across a slot of height 1 m, $Pr/Ra_h^{1/4} = 0.0046$, which is well within the upper limit predicted by condition 40. In this case the slot width given by

$$l^* = l_s\left(\frac{\kappa\nu h^*}{\alpha^* g\,\Delta T^*}\right)^{1/4} \tag{43}$$

at the onset of instability is 2.15 cm, whereas that given by Equation 41 is 2.85 cm. At the same temperature difference, the height would have to be reduced to about 42 cm before the vertical Rayleigh number Ra_h is small enough to ensure that the large-scale mechanism applies. Then the optimum slot width given by Equation 41 is about 2.30 cm.

References

1 Batchelor, G. K. Heat transfer by free convection across a closed cavity between vertical boundaries at different temperatures. *Q. J. Appl. Math.*, 1954, **12**, 209–233

2 Catton, I., Ayyaswamy, P. S., and Clever, R. M. Natural convection in a finite rectangular slot arbitrarily oriented with respect to the gravity vector. *Int. J. Heat Transfer*, 1974, **17**, 173–184

3 Lee, Y. and Korpela, S. A. Multi-cellular convection in a vertical slot. *J. Fluid Mech.*, 1983, **126**, 91–121

4 Daniels, P. G. Transition to the convective regime in a vertical slot. *Int. J. Heat Mass Transfer*, 1985, **28**, 2071–2077

5 Daniels, P. G. Convection in a vertical slot. *J. Fluid Mech.*, 1987, **176**, 419–441

6 Blythe, P. A., Daniels, P. G., and Simpkins, P. G. Thermal convection in a cavity: The core structure near the horizontal boundaries. *Proc. R. Soc.*, 1983, **A387**, 367–388

7 Daniels, P. G. The horizontal boundary-layer structure for the convective regime in a laterally heated vertical slot. *Q. J. Mech. Appl. Math.*, 1987, **40**, 257–277

8 Gill, A. E. The boundary-layer regime for convection in a rectangular cavity. *J. Fluid Mech.*, 1966, **26**, 515–536

9 Blythe, P. A. and Simpkins, P. G. Thermal convection in a rectangular cavity. *Physico-Chemical Hydrodynamics*, vol. 2 (D. B. Spalding, Ed.), Advance, New York, 1977, 511–524

10 El-Sherbiny, S. M., Raithby, G. D., and Hollands, K. G. T. Heat transfer by natural convection across vertical and inclined air layers. *J. Heat Transfer*, 1982, **104**, 96–102

11 Korpela, S. A., Lee, Y., and Drummond, J. E. Heat transfer through a double pane window. *J. Heat Transfer*, 1982, **104**, 539–544

12 Mizushima, J. and Gotoh, K. Nonlinear evolution of the disturbance in a natural convection induced in a vertical fluid layer. *J. Phys. Soc. Japan*, 1983, **52**, 1206–1214

13 Vest, C. M. and Arpaci, V. S. Stability of natural convection in a vertical slot. *J. Fluid Mech.*, 1969, **36**, 1–15

14 Gill, A. E. and Kirkham, C. C. A note on the stability of convection in a vertical slot. *J. Fluid Mech.*, 1970, **42**, 125–127

15 Korpela, S. A., Gozum, D., and Baxi, C. B. On the stability of the conductive regime of natural convection in a vertical slot. *Int. J. Heat Mass Transfer*, 1973, **16**, 1683–1690

16 Bergholz, R. F. Instability of steady natural convection in a vertical fluid layer. *J. Fluid Mech.*, 1978, **84**, 743–768